Final report

FOCAL PLANE ARRAY TECHNOLOGY FOR IR DETECTORS

Contract No SPC-95-4048

June 1996

Issuing Organization and Point of Contact

Institute of Physics, Charles University, Prague
Ke Karlovu 5, 121 16, Prague 2, Czech Republic
phone: (+42 2) 21911344, fax (+42 2) 296764, e-mail hoschl@karlov.mff.cuni.cz

REPORT DOCUMENTATION PAGE

Form Approved OMB No. 0704-0188

1. AGENCY USE ONLY (Leave blank)	2. REPORT DATE	3. REPORT TYPE AND DATES COVERED
	June 1996	Final Report

4. TITLE AND SUBTITLE

Focal Plane Array Technology for IR Detectors

5. FUNDING NUMBERS

F6170895W0366

6. AUTHOR(S)

Prof. Pavel Hoschl

7. PERFORMING ORGANIZATION NAME(S) AND ADDRESS(ES)

Charles University/Institute of Physics
Ke Karlovu 5
121 16 Praha 2 CZ 121 16
Czech Republic

8. PERFORMING ORGANIZATION REPORT NUMBER

N/A

9. SPONSORING/MONITORING AGENCY NAME(S) AND ADDRESS(ES)

EOARD
PSC 802 BOX 14
FPO 09499-0200

10. SPONSORING/MONITORING AGENCY REPORT NUMBER

SPC 95-4048

11. SUPPLEMENTARY NOTES

12a. DISTRIBUTION/AVAILABILITY STATEMENT

Approved for public release; distribution is unlimited.

12b. DISTRIBUTION CODE

A

13. ABSTRACT (Maximum 200 words)

This report results from a contract tasking Charles University/Institute of Physics as follows: Provide an annotated bibliography of research and development projects undertaken by the Czech Republic during the past 10 years in focal plane array technology for IR detectors in the 1-15 micrometer range.

14. SUBJECT TERMS

EOARD

15. NUMBER OF PAGES

25

16. PRICE CODE

N/A

17. SECURITY CLASSIFICATION OF REPORT	18. SECURITY CLASSIFICATION OF THIS PAGE	19. SECURITY CLASSIFICATION OF ABSTRACT	20. LIMITATION OF ABSTRACT
UNCLASSIFIED	UNCLASSIFIED	UNCLASSIFIED	UL

Final report
(draft)

FOCAL PLANE ARRAY TECHNOLOGY FOR IR DETECTORS

Contract No SPC-95-4048

June 1996

Issuing Organization and Point of Contact

Institute of Physics, Charles University, Prague
Ke Karlovu 5, 121 16, Prague 2, Czech Republic
phone: (+42 2) 21911344, fax (+42 2) 296764, e-mail hoschl@karlov.mff.cuni.cz

Distribution:

Dr.William Frederick — 1 copy
Associate Deputy for Sensors
Ballistic Missiles Defense Organization
The Pentagon
Washington, D.C. 20301-7100
U.S.A

Ms Victoria Cox — 1 copy
Liaison Officer
European Office of Aerospace Research and Development
(EOARD)
223/231 Old Marylebone Road
London NW1 5TH UK
United Kingdom

CONTENTS:

1. Introduction

Research of II-VI Compounds in our Institute was performed during a period of about three decades.

Materials: II-VI Bulk Crystals

CdTe, CdSe, CdS, CdO, ZnTe, Cd(SSe)

Continue:	(HgCd)Te, (CdZn)Te

Crystal growth:

Vertical Bridgman Method (VBM), Horizontal Bridgman Method (HBM), Vertical Zone Melting (VZM), Vapour Phase Transport Method (VPTM), Travelling Heater Method (THM)

Continue:	Bridgman Growth from Melt of Constant Composition (BGCC)		(HgCd)Te,
	Vertical Gradient Freezing (VGF)	-	(CdZn)Te

Transport properties:

C-V characteristics

Continue	Galvanomagnetic properties:	T:	2-300K,	B:	0-14T
	Thermoelectric properties:	T:	10-300K		

Optical properties:

FT - IR optical spectroscopy: T: 4.2-300 K

FT - IR magnetooptical spectroscopy: T: 10 K, B: 0-5 T

Continue	Photoluminescence:	T: 4.2-300 K
	Magnetophotoluminescence:	T: 10 K, B: 0-5 T.

II-VI Devices:

Cd(SSe)	photo camera - VIS detectors	Pentacon , Dresden (East Germany)
(CdZn)Te	γ-ray detectors	IAEA , Wien (Austria)
(HgCd)Te	PV IR detectors (8-14 μm)	Tesla Rožnov (Czech Republic)

Type conversion of p-(HgCd)Te

Ion Implantation		B, E ~ 100 keV, $3.10^{13}cm^{-2}$
continue	Ion Milling	Ar , E ~ 500 eV
	Reactive Ion Etching	Ar, CH_4/H_2
	Electron Beam Induced Current - EBIC	

2. Crystal Growth

2.1 (HgCd)Te

The principle of our proposed method, that we use for single crystal growth of (HgCd)Te, is shown in Figs.2.1-2.2. Our Bridgman growth from melt of constant composition (BGCC) is based on a demand to ensure melt of constant composition x_L above the crystal during the growth. The missing CdTe is transported to the phase boundary I_{mc} by diffusion from a suitable source during the whole process of growth. The process of growth was modelled supposing that the dominating transport process in the melt is diffusion. Following parameters were determined: ΔT for hot zone, diffusion coefficient D_{CdTe} of CdTe in HgTe from the profile of axial composition of quickly cooled melt. Results of measurements of axial/radial homogeneity are evident from Figs 2.4 and 2.5.

In the next period we plan to continue mathematical modelling of growth process of single crystals connected with experimental verification of theoretically calculated optimal growth parameters.

2.2 (CdZn)Te

Epitaxial technologies of (HgCd)Te growth are not available for us now, mainly from financial reasons. Therefore we decided, that our contribution to the technology of high quality MCT epitaxial layers for focal plane arrays can be the growth of high quality substrates on the basis of $Cd_{1-y}Zn_yTe$ (y = 0.03 - 0.06). With the help of Shubnikov method (Vertical Gradient Freezing) we are able to prepare high purity single crystalline ingots with diameter up to 10 cm and weight ≈1.5 kg oriented in {111} direction. The

boule axis is inclined at 1-3 ° to the {111}direction. The crystals with both types of conductivity can be prepared.

Table I - parameters of (CdZn)Te samples

	concentration (300K) (cm^{-3})	mobility (300K) (cm^2/Vs)	transmittance at 10 μm (300K)	dislocation density (cm^{-2})
n-type	1.10^{14}	920	0.64-0.66	5.10^4
p-type	1.10^{14}	85	0.64-0.66	5.10^4

Starting elements Cd, Zn, Te with purity 6N were produced in Czech Republic (Institute of Metals, Panenské Břežany).

Photoluminescence can be used for characterization and identification of point defects in (CdZn)Te substrates. An example of the spectrum measured on a sample grown in our Institute is shown on Fig.2.6. The spectrum is compared with the similar one taken on standard comercionally available substrate material from Johnson-Matthey Electronics [1] on Fig 2.7. Transmittance spectra in the spectral range 2.5-25 μm are on Fig.2.8.

Using double crystal diffractometry (DCD), X-ray rocking curves on (111) oriented (CdZn)Te have been tested on several samples. Results of these measurements are evident from Fig.2.9. Good microstructure was observed, the value of FWHM was about 15 arcsec (when 2 mm^2 spot size was used).

This year we plan to start test modelling of growth process of large volume single crystals, which can help to optimize expensive growth experiments. Also we would like to study native point defects in (CdZn)Te including those incorporated during

(a) the **growth process** (three solid phase transitions probably exist is solid state stability region during cooling, that can determine the precipitation and generation of native point defects)[2]. We plan to prepare single crystals, where various cooling speeds will be used after solidification of the ingot

[1] J.Lee and N.C.Giles, J.Appl.Phys.78, 1191 (1995)
[2] Yurii M.Ivanov, J.Crystal Growth, 4501 (1996)

(b) subsequent **thermal annealing.** In this case high temperature defect structure of (CdZn)Te can be frozen-in during fast cooling to room teperature.

Experimental methods: Hall effect, luminescence, positron annihilation, electron microscopy

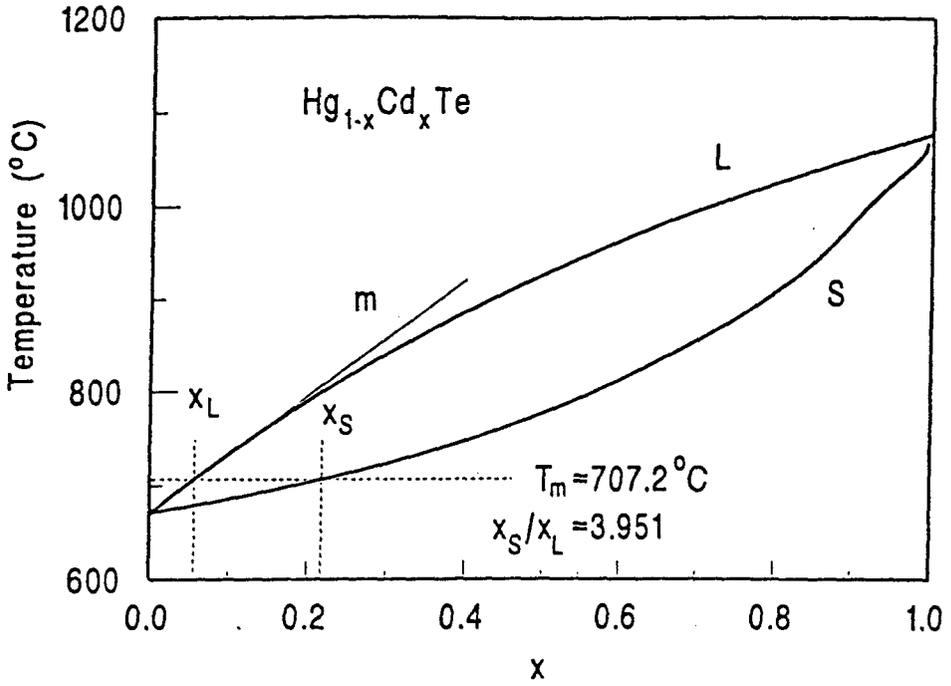

Fig.2.1 Pseudobinary HgTe-CdTe T-x phase siagram (m is the slope of the liquidus curve at $x=x_L$)

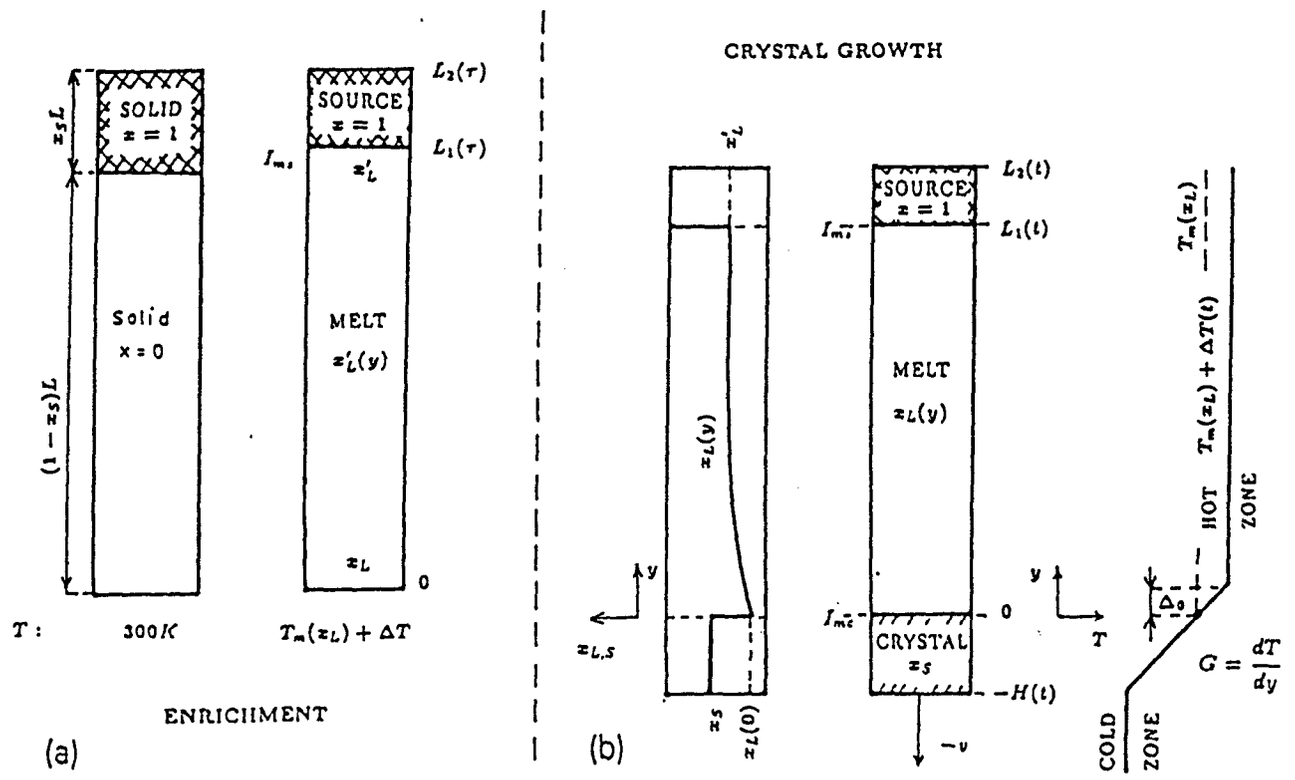

Fig.2.2 Schematic representation of one-dimensional model of (a) enrichment of melt and (b) crystal growth

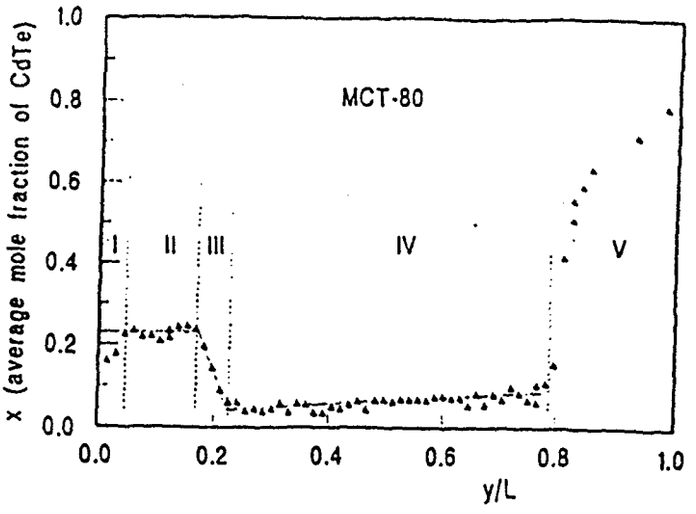

Fig.2.3 Axial distribution of the average composition in the ingot which is quenched to room temperature during growth

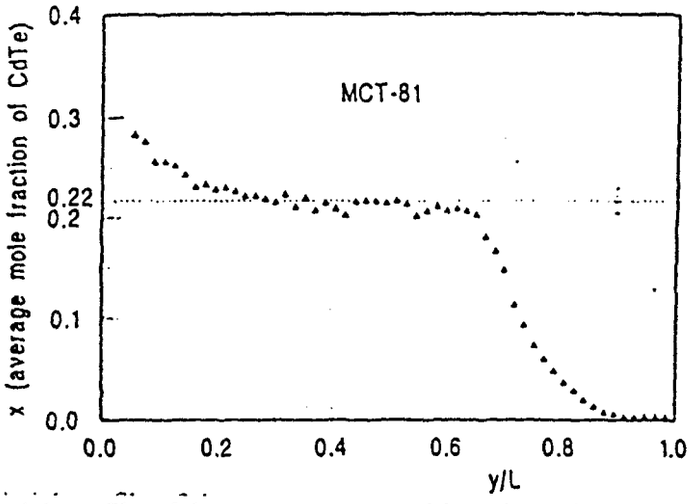

Fig. 2.4 Axial profile of the average composition along the quenched ingot

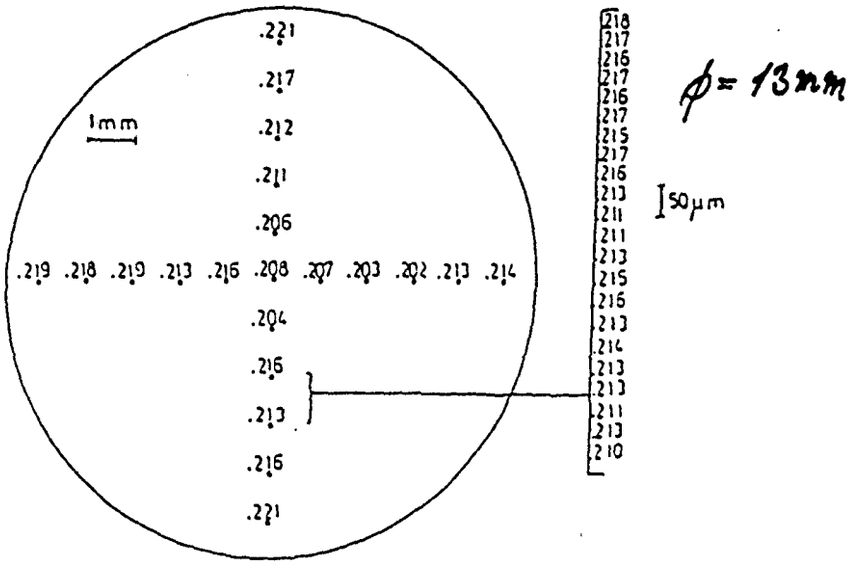

Fig. 2.5 Radial distribution of the composition across a wafer

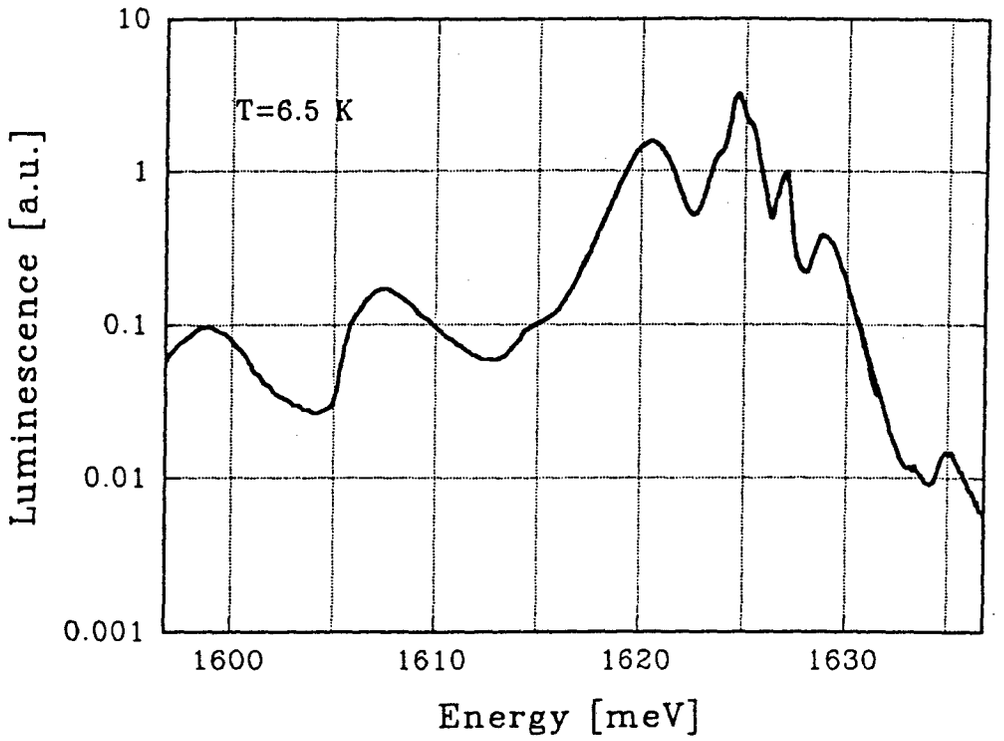

Fig 2.6 Luminescence spectrum of our (CdZn)Te sample measured at T=6.5K.

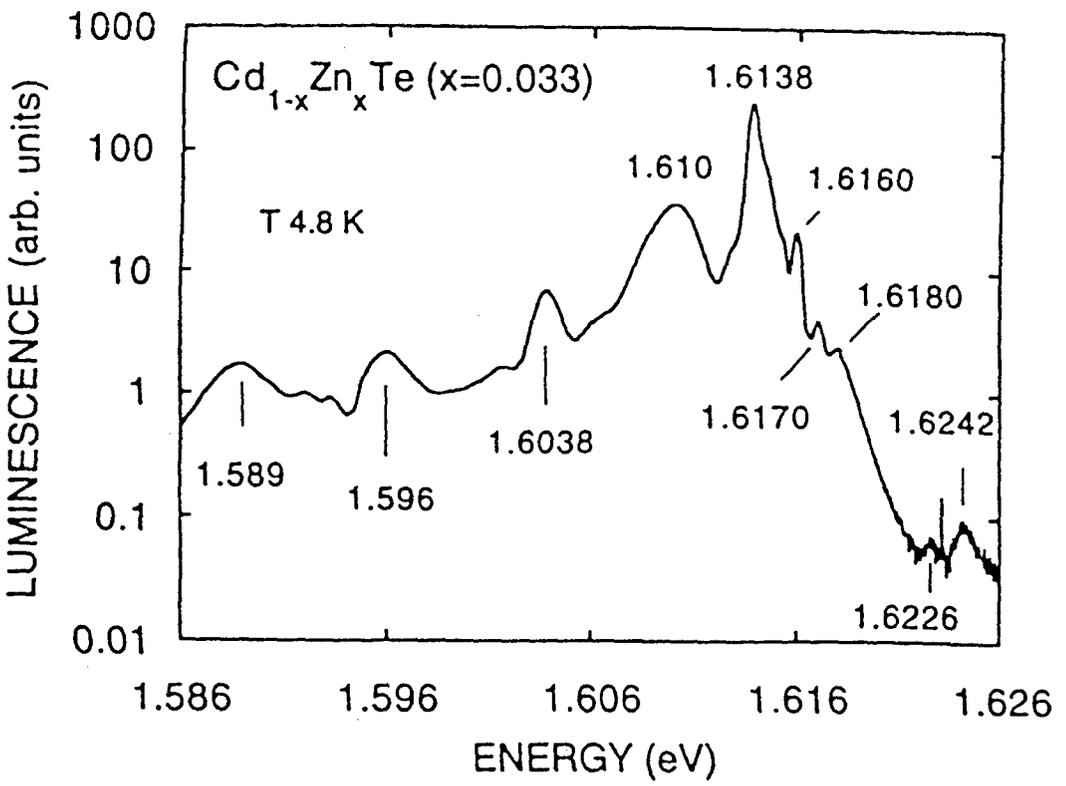

Fig. 2.7 Luminescence spectrum of (CdZn)Te from Johnson - Matthey Electronics, Spokane, WA as reported by J.Lee and N.C.Giles: J.Appl.Phys.78, 1191 (1995)

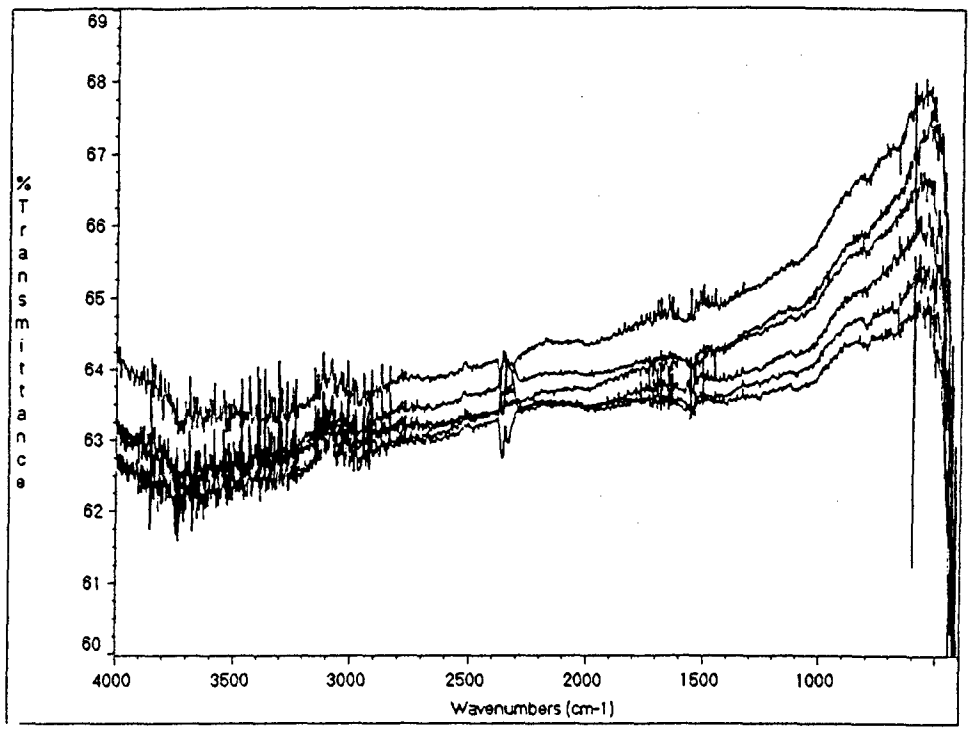

Fig.2.8 Transmittance of 3mm thick (CdZn)Te wafer

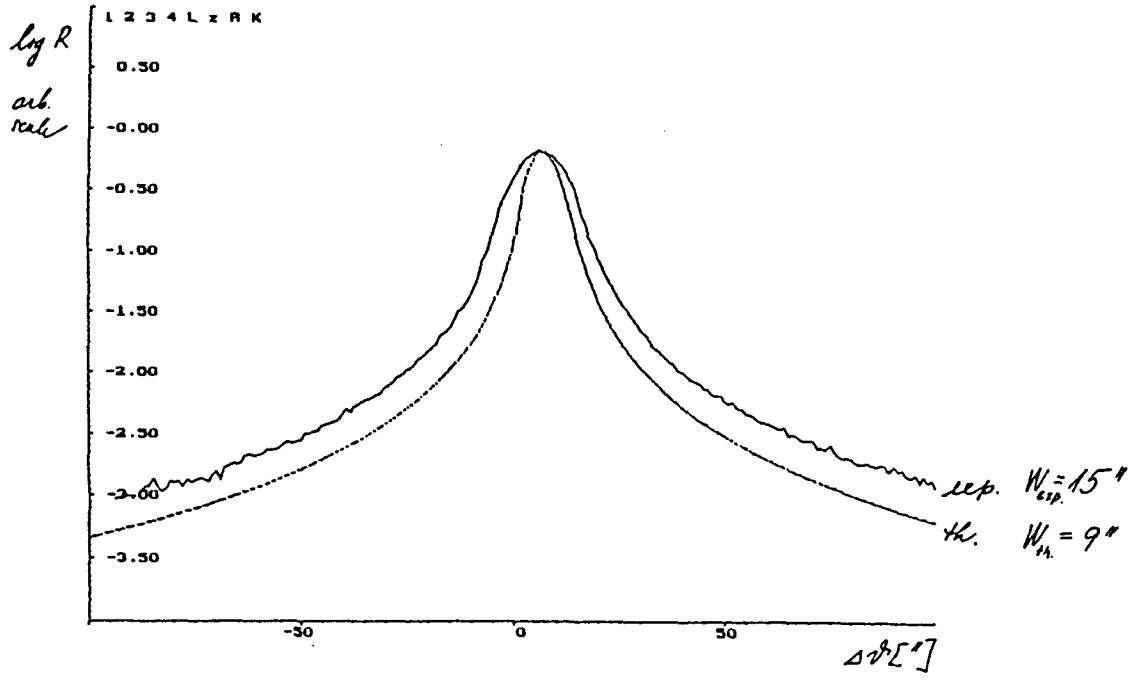

Fig. 2.9 X-ray rocking curves (CuK_α radiation) obtained in the middle of CdZnTe slice. W_{exp} and W_{th} indicate full widths at half maximum of experimental and theoretical curve, respectively.

3. Transport Properties

We have suggested a detailed model for evaluation of (a) concentrations of electrons, heavy and light holes, acceptors and donors, (b) mobilities of electrons, heavy and light holes; (c) lifetimes of excess carriers. The model is experimentally verified by galvanomagnetic measurements of (R_H, ρ) in the temperature range 2-300K and by EBIC measurements in the temperature range 140 - 300K and enables to determine basic material parameters important for IR PC and PV devices.

The electronic Boltzmann transport equation (EBTE) is solved in a limit of weak external electric field, parallel temperature gradient and perpendicular magnetic field. The sample is assumed homogeneous and macroscopic without mesoscopic effects. The bands are spherical, heavy-hole band is parabolic and electron and light-hole bands as well as wave functions are described in **kp** approximation by Kane formulae. The interband scattering is involved. Main scattering mechanisms $Hg_{1-x}Cd_xTe$ (x~0.2) often discussed in literature are scattering by ionized impurities, compositional disorder and polar-optical phonon scattering. A limited influence have acoustic phonon scattering, electron-hole scattering, nonpolar-optical phonon scattering, piezoacoustic scattering, phonon drag. For the best of our knowledge the phonon drag was not observed in this material. We expect that the alloy character of the three compound material affects a strong scattering of acoustic phonons and consequently shortens their mean free path. Due to the nonelastic scattering on optical phonons the relaxation time approximation is not applicable for these mechanisms. The usual techniques to solve EBTE in this case are based on variational, difference equation or Monte Carlo methods. Especially at low temperatures difference equation method is more proper than variational one. Due to the time consuming calculations also Monte Carlo methods is not convenient to use for the low field transport. Solving EBTE for the valence band of $Hg_{1-x}Cd_xTe$ (x~0.2) the transport in the light hole band is to be included. Using standard models of the light-hole scattering the calculated light-hole mobility exceeds significantly the values estimated from experimental data. This discrepancy is caused by strong scattering of the light holes into the heavy-hole band and consequently by collisional broadening of the light-hole band. The effect cannot be described within the limits of EBTE where the δ function like shape of spectral function inhibits collisional renormalization of the band structure. We propose a better approach to the transport in the light hole band based on a nonequilibrium

Green function formalism. The electron mobility calculated in MCT agrees well with experimental data obtained on n-type samples. On the other way p-type samples with similar x and impurity concentrations result to mobility significantly depressed. This discrepancy cannot be explained by a contingent compensation of the p-type material because the high heavy-hole mobility points to low impurity concentration. The electron-hole scattering is also not sufficient. Consequently we ought to presume an additional scattering mechanism present in these samples which is not discussed currently in literature. The transport properties of standard samples are often influenced by a transport on surface degenerated states (SDS). These states originate from a fast oxidization of etched samples or passivation. Decreasing temperature of p-type samples below ~ 10K the free carriers freeze out and transport in SDS prevails. As it was observed SDS exhibit n-type - inversion layer - as well as p-type - accumulation layer - character. Similar identification on n-type samples is not so easy. The n-type samples are typically degenerated and bulk transport prevails above SDS at all temperatures. The combination of the two transport channels displays in this case at a measured effective mobility which is due to low mobile SDS lowered against pure bulk one. In all cases SDS are convenient to be studied by magnetic field transport measurements.

Within the temperature range approx. 50-300K the bulk properties, and within the range 2-50K the surface properties of samples are determined. Our results on p-(HgCd)Te coated with passivation layers are evident from Figs 3.1 and 3.2. In the first case (native sulphides + ZnS passivation layer) an inversion layer exists on the surface, Fig.3.2 depicts accumulated surface behavior (passivation - ZnS). Parameters of samples are evident from the Table II. We studied influence of (a) atmosphere, (b) ZnS passivation, (c) native sulphides + ZnS passivation.

The (HgCd)Te - anodic oxide interface was studied also by magneto-capacitance and magneto-conductance measurements of MIS structures. The occupancy of the 2D subbands in the inverted surface layer below the anodic oxide and density of interface states as a function of their energy were determined. From the carrier freeze-out below ≈15 K the acceptor band activation energy was found.

In the case of interest, we are able to continue in this research, e.g. to study silicon nitride or another passivation layer on our single crystals or on epitaxial layers prepared on our (CdZn)Te substrates.

Table II - Surface parameters of (HgCd)Te samples

R_H is the Hall constant, μ_s is the the mobility of surface carriers and c_s is the surface charge

Sample No	Passivation	Days after passivation	R_H at 6K (cm^3C^{-1})	μ_s (cm^2/Vs)	c_s $10^{12}(cm^{-2})$
501203	native oxide	1	$-2x10^6$	1300	0.08
		180	$-1x10^5$	4000	2
		330	$-6.5x10^4$	3500	3.5
5006B5	native oxide	4	$3.2x10^4$	215	10
		11	$1x10^4$	310	26
		39	$6x10^3$	315	53
		60	$1.8x10^3$	260	120
6408A3	ZnS	2	$9.0x10^3$	260	36
		80	$2.8x10^3$	74	120
6408A4	native sulf.	9	$-3.3x10^4$	-	-
		80	$-1.0x10^3$		
		180	$2.6x10^3$		
6408A5	native sulf. + ZnS	10	$-4.7x10^4$	1500	7.2
		73	$-1.1x10^4$	3600	2.85
		160	$-1.4x10^4$	5500	2.14
		330	$-1.8x10^5$	4300	1.71

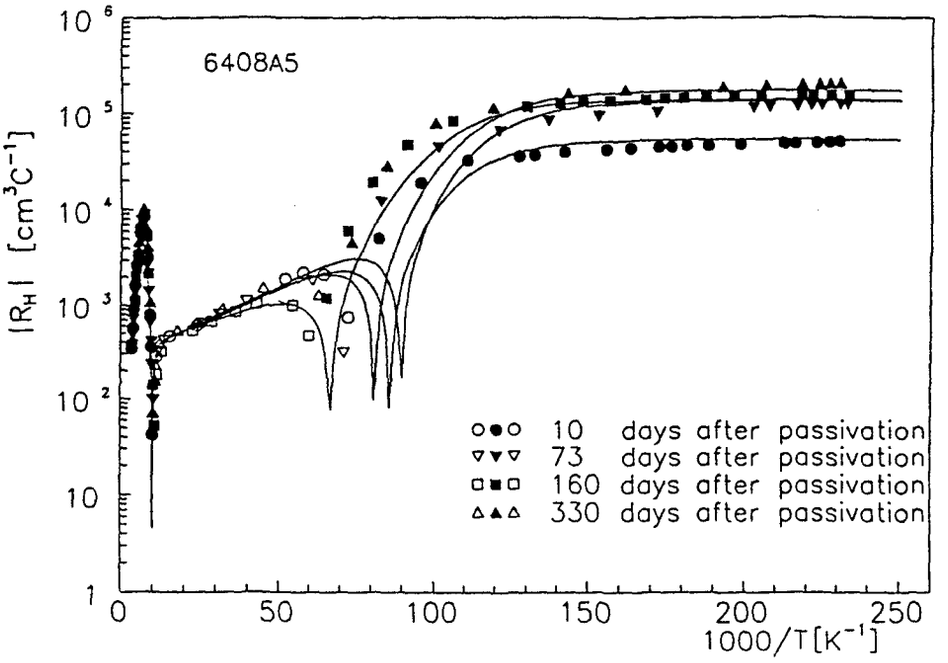

Fig. 3.1 Temperature dependence of the Hall coefficient. Passivation: native sulphides + ZnS, full symbols $R_H<0$, open symbols $R_H>0$.

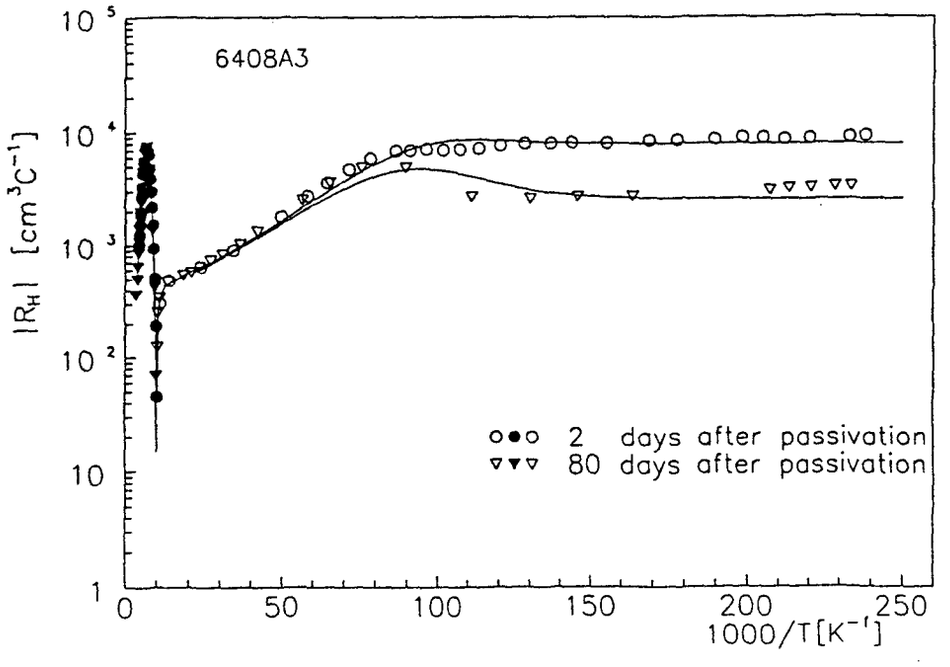

Fig. 3.2 Temperature dependence of the Hall coefficient. Passivation: ZnS, full symbols $R_H<0$, open symbols $R_H>0$.

4.Optical Properties

Very early studies of bulk (HgCd)Te crystals were devoted to interband Faraday rotation and its dependence on the composition x. The interband Landau level transitions were then investigated on photoconductive and photovolatic samples of (HgCd)Te with x about 0.2 by adapting Fourier Transform IR Spectroscopy. The coexistence of the oscillatory photoconductivity due to hot electron - LO phonon relaxation with Landau level oscillations shown on Fig. 4.1 was observed on appropriate samples. From magnetophotoconductivity experiments, the activation energy of shallow acceptors and of two deep levels in the gap of (HgCd)Te could be determined (see Fig.4.2).

The optical absorption edge of various (HgCd)Te samples has been thoroughly investigated. Three types of samples with characteristic slope of the exponential edge could be selected (see Figs. 4.3 and 4.4). The edge in the samples with the highest measured slope is formed by interaction with acoustic and LO - optical phonons, whereas the lower slope edge is formed by the impurity and defect induced static disorder. The best samples were used for detailed study of the temperature dependence of the gap E_G by optical absorption and the Hall efect measurements. The observed shift has been compared with various published semi-empirical relations describing the composition and temperature dependence of the gap. The E_G was determined exactly from magneto-optical measurements at low temperature and its change with temperature was measured as a shift of the absorption edge. The measured dependence is in the best agreement with the relation published by Seiler et al. in J.Vacuum Sci.Technol. **A8**, 1237 (1990) with slightly modified temperature coefficient.

The refractive index n of (HgCd)Te was measured as a function of composition for x in the range x = 0.18 - 0.52 at 80 K and room temperature. Based on these measurements, the empirical formula enabling to calculate n for any x were derived by fitting the compositional dependence of the Sellmeir coefficients.

An experimental set up for luminescence and magnetoluminescence studies in the near IR region has been built up recently. This equipment will be used for characterization and identification of point defects in (CdZn)Te substrates. An example of the measured spectrum is shown in Fig. 2.6

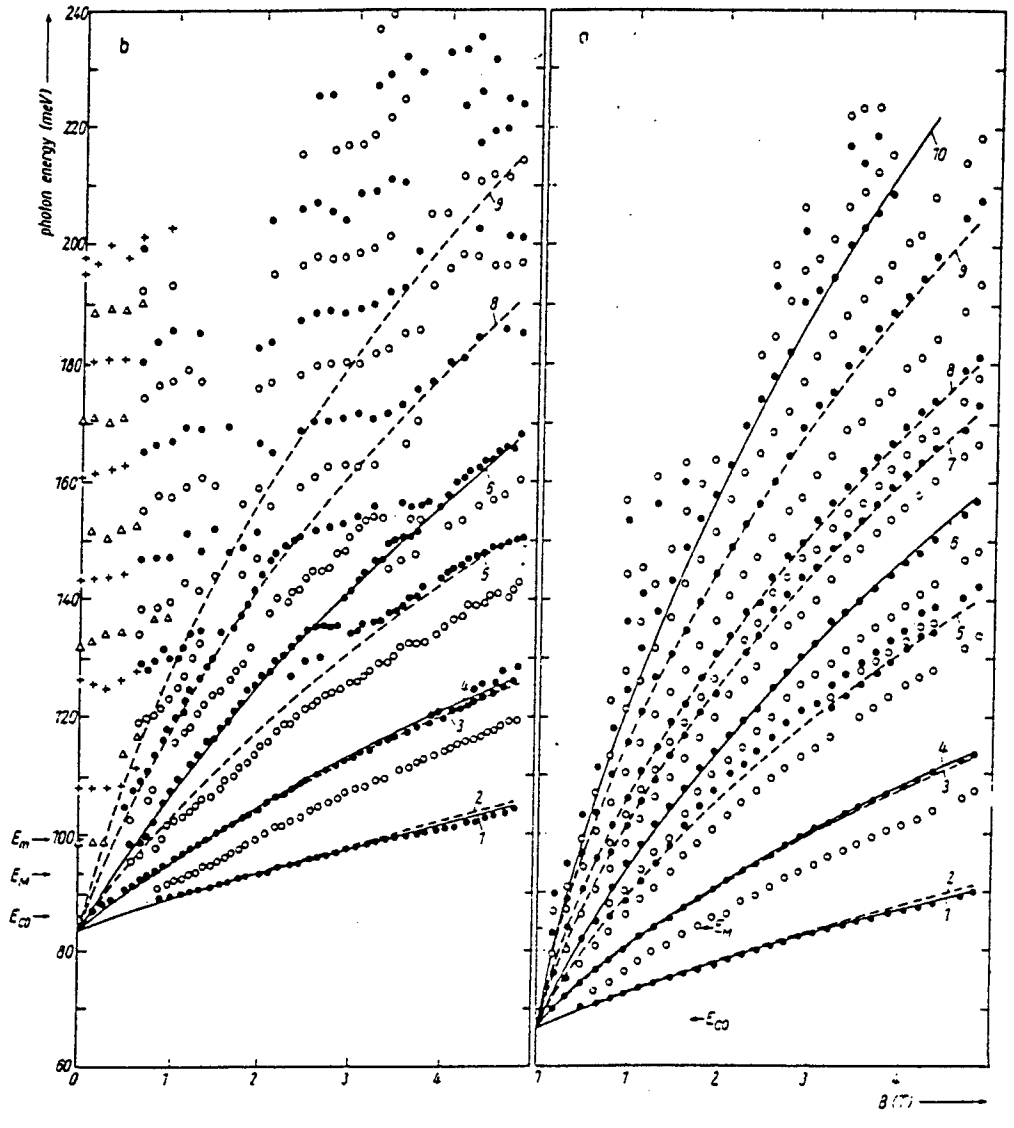

Fig. 4.1 Extrema in the relative photoresponse curves as a function of the magnetic field at 10K. The solid lines are obtained by fitting the data with the quasi - Ge model. The coexistence of the LO-phonon oscillatory photoconductivity with Landau level oscillations is clearly seen.

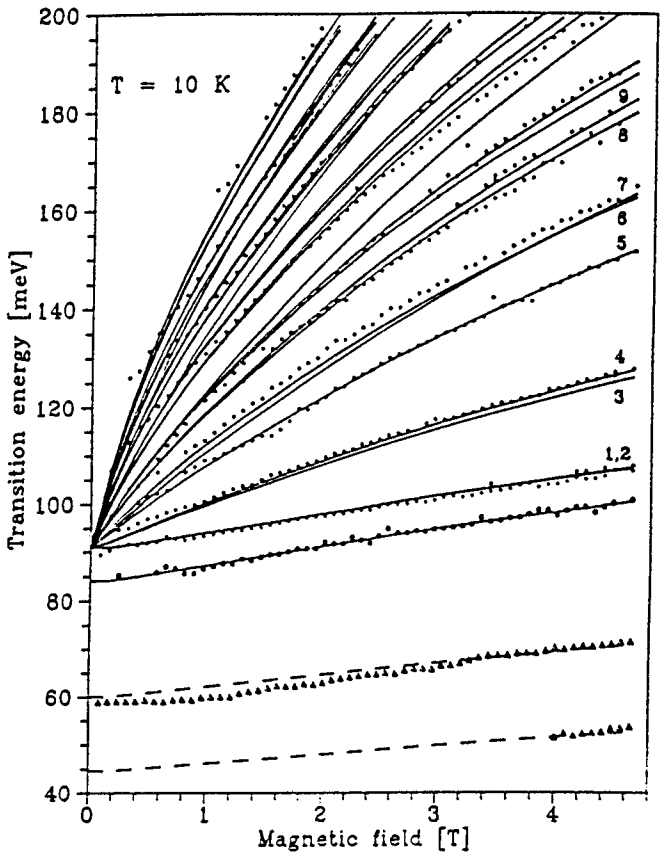

Fig. 4.2 Fan chart plot of transition energies at 10K versus magnetic field. Solid lines denote calculated curves for interband transitions. The determined sample parameters: composition x = 0.217, E_a = 7 meV, deep levels - E_{D1} = 0.49 E_G, E_{D2} = 0.66 E_G

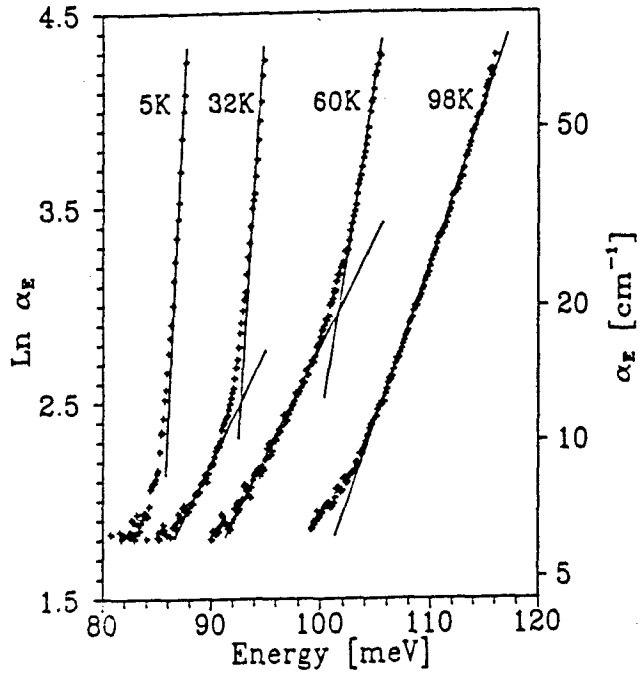

Fig. 4.3 Semilogarithmic plot of the edge absorption coefficient at various temperatures for the sample of Type I.

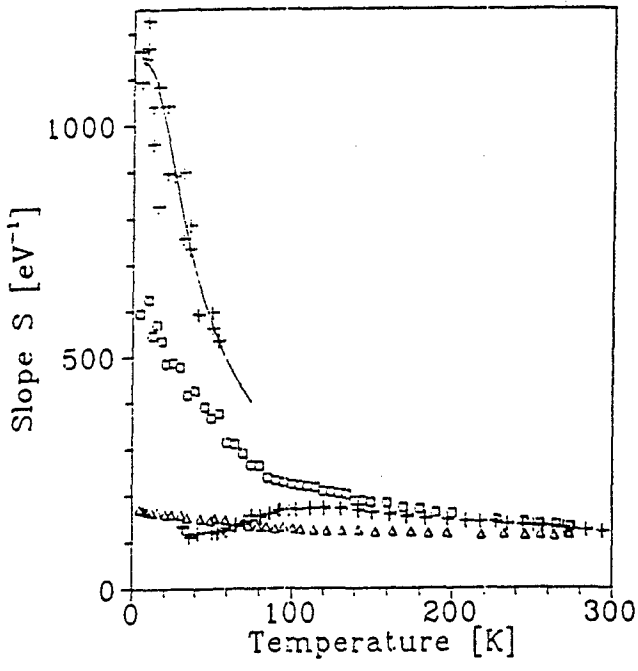

Fig. 4.4 Slope S(T) as a function of temperature. Crosses, squares and triangles correspond to samples of types I,II and III, respectively. The solid line is the best fit of the experimental data.

Type I: the maximum slope S(5K) $\approx 1200 eV^{-1}$
low concentration p-type, x=0.226, $p \approx 1.5 \times 10^{15} cm^{-3}$

Type II: the maximum slope S(5K) $\approx 600 eV^{-1}$
low concentration p-type, $p \approx 1.5 \times 10^{15} cm^{-3}$, $\mu_h(30K) > 1000 cm^2 V^{-1} s^{-1}$

Type III: the maximum slope S(5K) $\approx 200 eV^{-1}$
higher concentration p-type, $\mu_h(30K) \approx 700\ cm^2 V^{-1} s^{-1}$

5.Ion Milling and Reactive Ion Etching of p-(HgCd)Te

We studied influence of various dry etching methods (ion milling with low energy Ar ions and reactive ion etching in Ar and CH_4/H_2) on transport properties of (HgCd)Te. These dry etching methods result not only in a desired removal of front part of the sample, but also in drastic and very deep changes in its transport properties. As a consequence, p-type samples are usually converted to n-type and the created p-n junction can reach depth ≈100 μm. We studied the p-n junction depth by electron beam induced current method (EBIC). A mixed secondary electron and EBIC micrograph is shown on Fig.5.1 (part of the sample was protected from the stream of incident Ar ions by a photoresist mask). We can see a homogeneous diffusion profile. We developed a model to explain this unusually fast diffusion that occurs at room temperature. The model is based on the assumption, that during ion milling Hg interstitials are created at the sample surface. Part of the interstitials then diffuse into the sample, where they recombine with mercury vacancies (basic defects in p-(HgCd)Te). After then residual foreign n-type defects start to dominate and convert the material to n-type. Dependence of the p-n junction depth on temperature at which ion milling was performed (77-300K) is depicted in Fig.5.2. It is evident, that p-n conversion of (HgCd)Te is a temperature activated process. Theoretical modelling of this temperature dependence yields 120 meV as a migration energy of Hg interstitials. Results of this experiment also show, that it is possible to avoid undesirable p-n conversion by cooling of the substrate to 77K.

We also studied p-n conversion occurring during reactive ion etching (RIE) of (HgCd)Te in Ar and CH_4/H_2. For H_2/CH_4 RIE experiments two samples with a different composition and hole concentration ($x \approx 0.21$, $p = 1x10^{16}$ cm^{-3}, $x \approx 0.28$, $p = 5x10^{15}$ cm^{-3}) were used. The following process parameters were applied: Etch time = 10 minutes, rf-power = 180 W, dc bias ≈ 300V and the H_2/CH_4 partial pressure ratio was changed keeping the total chamber pressure constant at 0.05 Torr. The dependences of the etch depths and p-n junction depths vs partial pressure of H_2 and CH_4 for both samples are shown in Fig.5.3 and 5.4, respectively. The etch depth as a function of the partial pressure of H_2 and CH_4 is practically identical for both samples. On the other hand the p-n junction depth decreases with increasing methane fraction in the mixture. The different hole concentrations in the two samples are causing the different value of the p-n junction depth. It was found that

H_2/CH_4 RIE processes etch p-(HgCd)Te and create an n-type layer under an etched surface for any gas ratio (also for pure gases).

The p-n junction and etch depth as a function of time, Ar pressure and rf-power were investigated for samples with the hole concentration $p=1x10^{16}$ cm^{-3}. Fig. 5.5 shows the p-n junction and etch depths versus etch time (etching parameters: Ar pressure = 0.05 Torr, rf-power = 180W, dc bias ≈ 300V). The etch depth depends linearly on time but the p-n junction depth increases proportional to $t^{0.52}$. This behaviour coresponds to our theoretical model for ion milling with Ar ions Fig.5.6 shows the p-n junction and etch depth as a function of Ar pressure (etching parameters: etch time = 10 minutes, rf-power = 180W). It can be seen that both depths reach a maximum at about 0.1 Torr.

The results of the presented experiments show that RIE in all kinds of the examined plasma conditions is suitable for dry etching of p-(HgCd)Te but an n-type layer is always created under the etched surface over a considerable distance (≈10-100μm).

It seems reasonable to assume, that the mechanism responsible for the p-n conversion is the same as that observed during ion milling with Ar ions. Accelerated plasma ions sputter the (HgCd)Te surface, liberate Hg atoms from ordinary lattice positions and create a source of Hg interstitials under the etched surface. Some part of these atoms diffuse quickly into the material, where they decrease the concentration of acceptors by interaction with point defects, mainly Hg vacancies. Residual or native donor impurities then start to dominate in the conductivity and cause the p-n conversion. The depth of the p-n junction depends on the type of used plasma. .

Based on our results, the H_2/CH_4 and Ar RIE processes cannot be recommended for the substrate etching and structuring of p-(HgCd)Te at room temperature because both processes create an n-type layer under the etched surface. It was found that the lowest electrical damage during H_2/CH_4 RIE was created at a low level of hydrogen in the mixture.

In the future we would like to study dynamics of defects created during ion milling and RIE by in situ measurements of resistivity and relaxation effects after finishing of the process. We would also like to study influence of passivation layers on surface recombination of carriers by EBIC method.

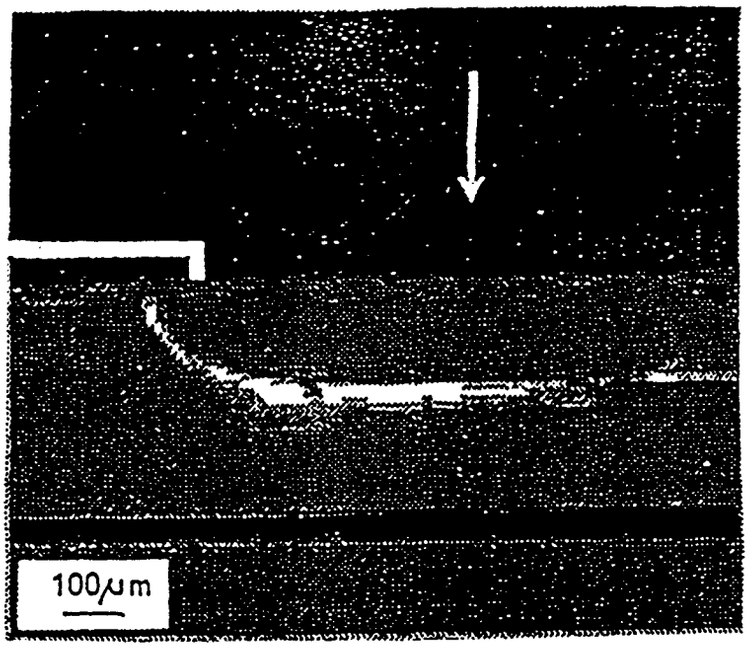

Fig. 5.1 A mixed EBIC-SE micrograph of sample 4913E6 cross section . The white solid line marks the position of the photoresist mask, the arrow indicates the direction of incident Ar ions.

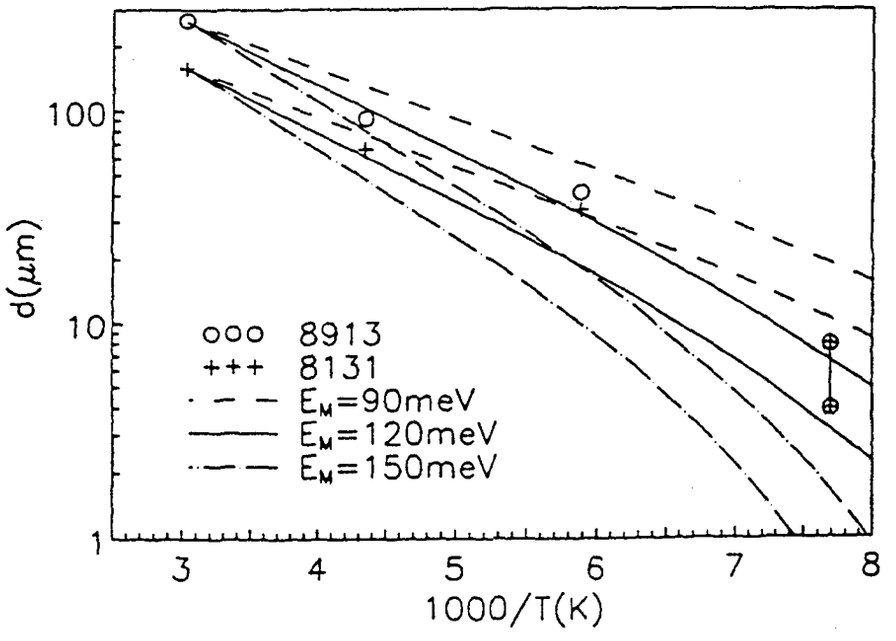

Fig. 5.2 Depths of the p-n junction of two sets of ion milled samples together with theoretical curves for various migration energies of mercury interstitials

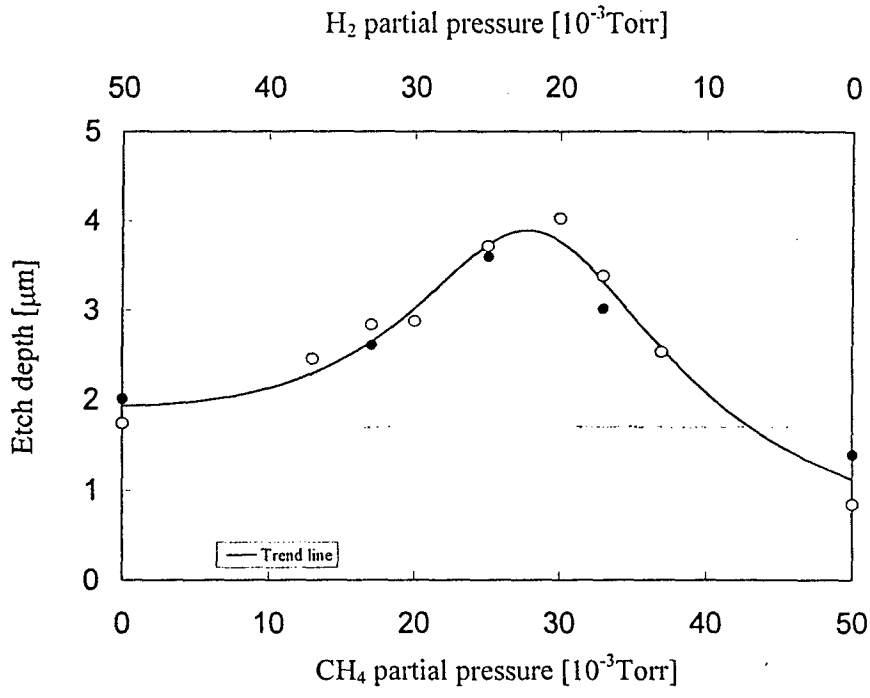

Fig. 5.3 Etch depth as a function of H_2 and CH_4 partial pressure (H_2/CH_4 RIE) (ooo: x~0.21, p=1x10^{16}cm^{-3}, ●●● x~0.28, p=5x10^{15}cm^{-3})

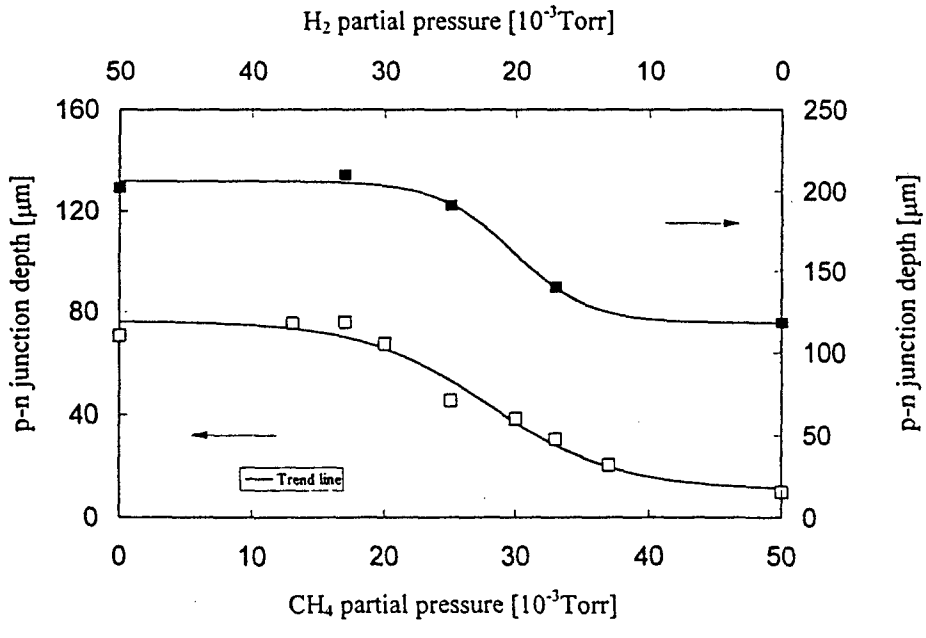

Fig. 5.4 p-n junction depth as a function of H_2 and CH_4 partial pressure (H_2/CH_4 RIE) (□□□: x~0.21, p=1x10^{16}cm^{-3}, ■■■ x~0.28, p=5x10^{15}cm^{-3})

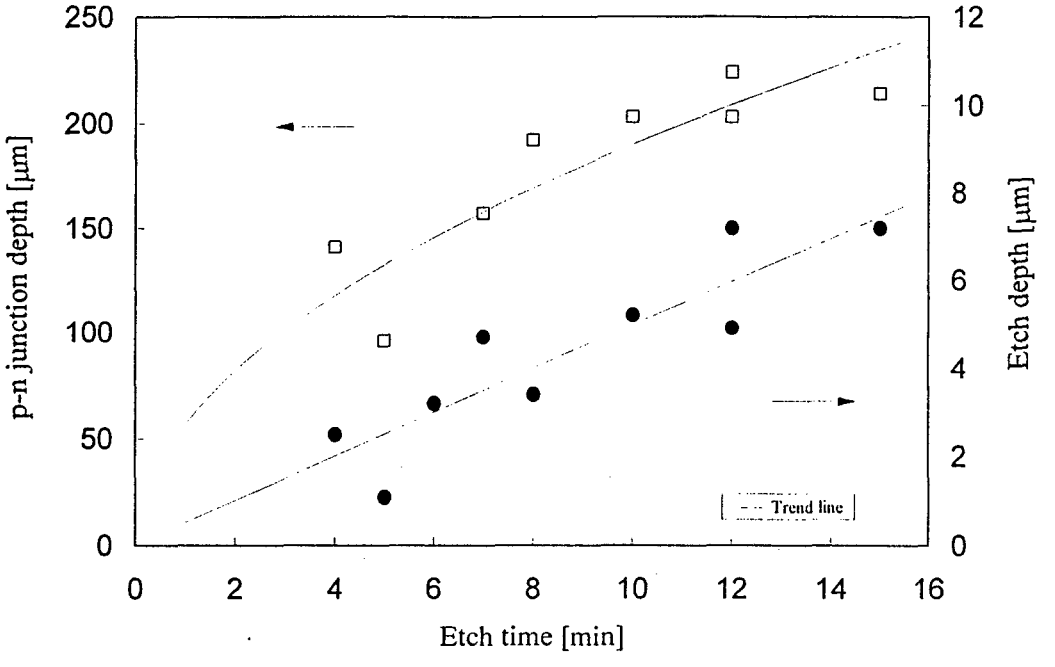

Fig 5.5 Etch depth and p-n junction depth as a function of etch time for a rf power of 180 W and an Ar pressure of 0.05 Torr (Ar RIE)

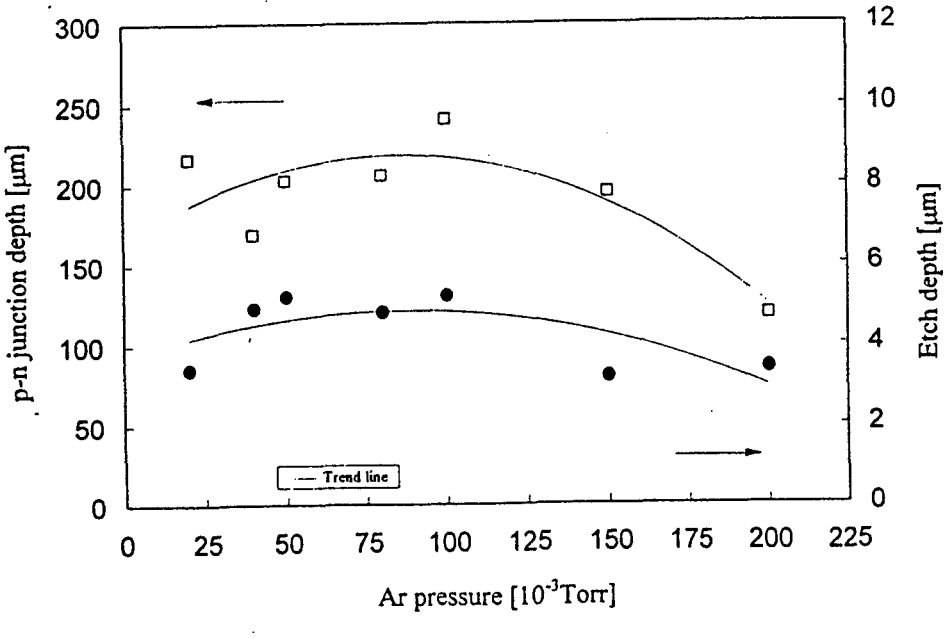

Fig.5.6 Etch depth and p-n junction depth as a function of Ar pressure for an etch time of 10 min and a rf power of 180 W

6.Summary

Based on the research we performed so far and on the knowledge obtained during the visit in SRII, SBRC/Hughes and Rockwell Research Center we plan to concentrate our next activities to:

I. Preparation of high quality and high purity (HgCd)Te and (CdZn)Te single crystals
II. Study of interaction of ions with (HgCd)Te and (CdZn)Te surface
III. Study of defects in (HgCd)Te and (CdZn)Te surface both generally and in connection with technological processes (points I and II)

Concretely following works will be performed:

1. Preparation of perfect (CdZn)Te single crystals with diameter up to 10 cm, modelling of the growth process. Optimalization of (CdZn)Te single crystal growth conditions
2. Study of defects generated during the process of growth of (CdZn)Te single crystals by galvanomagnetic (4.2 - 300K) and photoluminescence ($\approx$ 5K) measurements or positron annihilation.
3.Preparation of (CdZn)Te substrates in orientation (111) and (211) for LPE/MBE epitaxial growth to be provided to SBRC and Rockwell
4. Study of influence of defects and foreign impurities on mobilities of carriers on epitaxial layers p-(HgCd)Te (As) and n-(HgCd)Te (In) including determination of concentration of carriers, impurities and defects; explanation of influence of passivation layers with a possible study of their long-term stability (Rockwell)
5. Study of p-(HgCd)Te (As) - n-(HgCd)Te (In) junctions by EBIC method; determination of diffusion lengths of minority carriers, modelling of influence of various mechanisms that influence lifetime of minority carriers (Rockwell)
6. Study of influence of ion milling on properties p-(HgCd)Te(As) under the surface, eventually explanation of existing diffusion processes (SRII)